

1

Dynamic Pressure and Temperature Responses of Porous Sedimentary Rocks by Simultaneous Resonant Ultrasound Spectroscopy and Neutron Time-of-Flight Measurements

James A. TenCate, Timothy W. Darling, and Sven C. Vogel

1.1

Introduction and Background

Rocks are everywhere, yet there are still surprising puzzles about their peculiar dynamic elastic properties, especially their hysteresis, non-Hookean response, and rate-dependent behavior. Since before recorded history, mankind has been making dwellings, hammering out monuments, and even constructing huge buildings out of rock, for example, the famous Strasbourg Cathedral built in the Middle Ages is made almost entirely from Vosges sandstone. Nowadays, one extracts oil and gas from rocks, explores ways to store excess CO₂ in them, and tries to mimic their resilience and durability with concrete. The imperfect way in which mineral grains end up cemented into rocks dictates how fluids move in oil or gas reservoirs or in aquifers. Indeed, these very fluids are often a key mechanism for that cementation. The diagenesis of rocks, their formation, and cementation history are of great geological interest as well. Hence, the dynamic elastic properties of rocks have been a topic of continuing scientific study for well over a century.

To narrow the focus of this chapter, the subject is primarily the behavior of rocks that have commercial interest. These rocks may contain oil and gas, or might be considered as a reservoir for CO₂ storage. These rocks are primarily sedimentary, and the focus of this chapter will sharpen even more, dealing exclusively with sandstones. A sandstone is an imperfectly cemented collection of quartz grains, which is porous and permeable to fluids (which often play a key role in the cementation) and may contain significant amounts of clays and other materials. In the experiments described here, the rocks studied will be extremely pure and clean sandstones, 99+% pure SiO₂ formed from quartz (prehistoric, 77 MYBP) Aeolian beach sand, known as Fontainebleau sandstone. Such rocks are simply composed of the grains and cementation.

How does one describe and examine such a sandstone and how is it different from man-made materials? A thin section examined under a polarizing microscope can show the crystallographic orientation and the nature of the grains, bonds, and cementation. A thin section of Fontainebleau sandstone is shown in

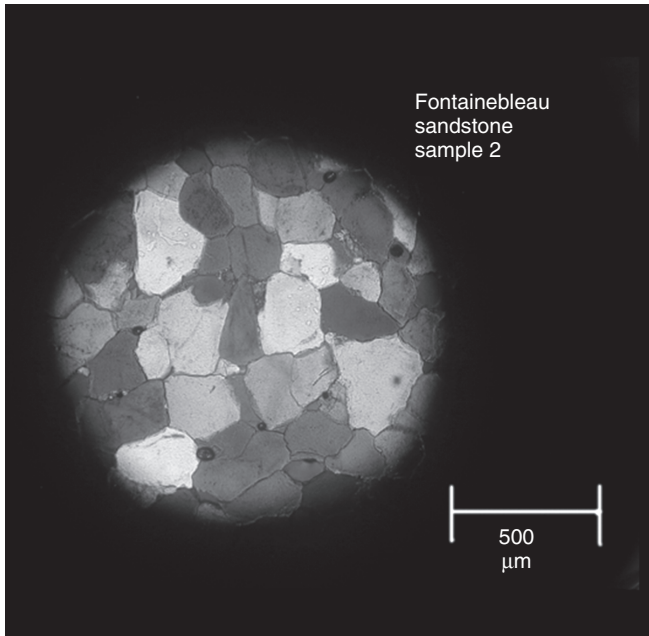


Figure 1.1 An image of a thin section of Fontainebleau sandstone in a polarizing microscope. The largely single crystal grains are rounded (convex) while porosity, filled with epoxy, has more concave boundaries. The largest visible grains are taken as

characteristic of the grain size, about $200\ \mu\text{m}$ across. With very porous rocks, the possibility of grain movement during polishing must be considered, possibly distorting apparent boundaries.

Figure 1.1. All the grains are roughly of the same size (about $150\text{--}200\ \mu\text{m}$), and none of the material in the section shown here has any significant polycrystalline components and very little of it is amorphous or glassy (which shows up as black under crossed polarizers). However, the reality is that a thin slice of a rock really does not give a very good representation of the porosity and permeability or even of the cementation. Care must be taken in extracting distributions of pore and grain sizes from sections, and often the cementation at grain contacts is difficult to identify. Amorphous cement, for example, can easily be missed and more advanced petrographic techniques such as cathodoluminescence or electron backscatter diffraction in an SEM must be used [1]. Occasionally, pore casts – where an epoxy is spun into the pore space and the sand dissolved away with an acid – are made to study the three-dimensional network of pores [2]. X-ray micro-CT images on very small samples are made as well, originally to provide an input for modeling, but similar to thin sections, they contain no information on the mechanical properties of the system. The contact network of grains, the pore space they can rotate into, and the fluids that can move around in that pore space (e.g., water, oil, and gas) all couple to the dynamics of a rock; direct measurements on the scale of these features is extremely difficult.

So the cementation, porosity, and permeability are important for many reasons: what can be done to study and understand how a rock is put together in a laboratory setting? The following lists several possible applied external fields [3] that will guide the experimental discussion that follows:

- 1) Pressure/stress
- 2) Temperature
- 3) “Humidity” resulting in the movement of fluid in a rock
- 4) Electric or magnetic fields
- 5) Vibration or acoustic energy.

The first two parameters, pressure — and the associated stress-strain measurements — and temperature — and the associated sound speed versus temperature measurements, seem to have been motivated by oil and gas exploration at the turn of the last century. “Humidity” measurements came out of interest in ultra dry lunar/moon rocks in the 1970s. Interest in electric and magnetic fields came a bit later and the last, vibration and acoustic energy, came later still. Vibration as an applied field is a bit unusual and is distinct from the use of a low amplitude stress wave to measure sound speed. “Vibration” has to do with changing the internal arrangement of strain fields with an acoustic AC drive — dubbed slow dynamics by TenCate and Shankland [4] — in contrast with the other DC applied fields. Other experiments and external fields may be possible. However, in this chapter just pressure and temperature measurements will be considered. These measurements are rate dependent and show a nonreversible response normally thought of as “hysteresis.” These are all “macroscopic” measurements, done at sample scales of a few to tens of centimeters. Some discussion of each kind of measurement is appropriate at this point before we delve into the combined macroscopic and atomic (neutron) measurements reported in the bulk of the chapter.

1.2

Macroscopic Measurements

1.2.1

Stress-Strain Measurements

The hysteretic macroscopic strain response of rocks to uniaxial compressive stress (force/unit area) has been noted since the turn of the last century [5]: after being brought to a “state of ease” (conditioning) by application of high stresses, most rocks display a repeatable curved, stress–strain loop under cyclic loading, for example, [6, 7]. Fully recoverable hysteretic processes, driven by stress and dependent on the previous extreme stress values, produce multiple values of strain for stresses between the cycle and values. The details of these processes (which produce similar effects in many different kinds of rocks) are usually ascribed to grain contact and fluid effects.

The literature reports a number of models to describe this hysteretic behavior, such as the Hertz–Mindlin model [8] and the Preisach–Mayergoyz (P–M) space model [9–11]. In analogy with magnetic domains in a magnetic system, a hysteretic rock “domain” or unit in the P–M scheme opens at one stress and closes at another. While these models can reproduce qualitatively the observed responses, assignment of the model systems to real physical elements has some problems, such as requiring frictional surface slip at interfaces in sandstone, where we expect small-area, perhaps brittle, bonds of a solid silicate. The tensile and shear strength of rocks, however, suggest that macroscopic slip cannot occur at every contact.

Rate effects have been reported and are worth noting. Claytor *et al.* [12] discovered that the *rate* at which hysteresis loops are taken is important for certain rock samples, especially sandstones. Elastic aftereffect, in analogy with magnetic aftereffect, is a process whereby hysteretic elements do not stay “switched” but snap back to some “relaxed” state. Thus, if a hysteresis loop is taken slowly enough, the area between the loops vanishes and the stress–strain curve is merely nonlinear. Figure 1.2 shows two stress–strain hysteresis loops taken from Claytor’s data: one quickly, 0.38 s between stress increments; and the other very slowly, over a weekend with 60 s between stress increments. The area within the error bars (not shown) is essentially zero for the very long stress–strain experiment. What physics is responsible? Fluids coupling to the rock grain skeleton could be one answer, and there may be many other possible explanations. There is simply not enough data on enough rocks yet to model how fluids couple to rock grains and affect the dynamics of a rock. (Reference to chapter by Jan Carmeliet.)

1.2.2

Temperature Variations

Macroscopic temperature measurements on rocks started to appear in the 1920s and 1930s. Although there are many measurements where sound speed (modulus) is measured as a function of temperature for a wide variety of crystal rocks, there are almost no reports of hysteresis in temperature measurements that we are aware of. Ide *et al.* [13] did some of the first measurements of temperature versus modulus/sound speed, dating back to the mid-1930s. His work was motivated by learning about the composition of the earth’s crust under combined high temperatures and pressures. Although Ide did reverse the temperature protocol several times during the course of his experiments, he was looking for permanent deformation and did not report any hysteresis in his temperature data. The research done by Ulrich and Darling [14], on the other hand, is one of the very few reported observations of large hysteresis temperature loops. Their work is interesting because the hysteresis loops were observed at very low temperatures that are typically found on planets other than the Earth (see also [15]).

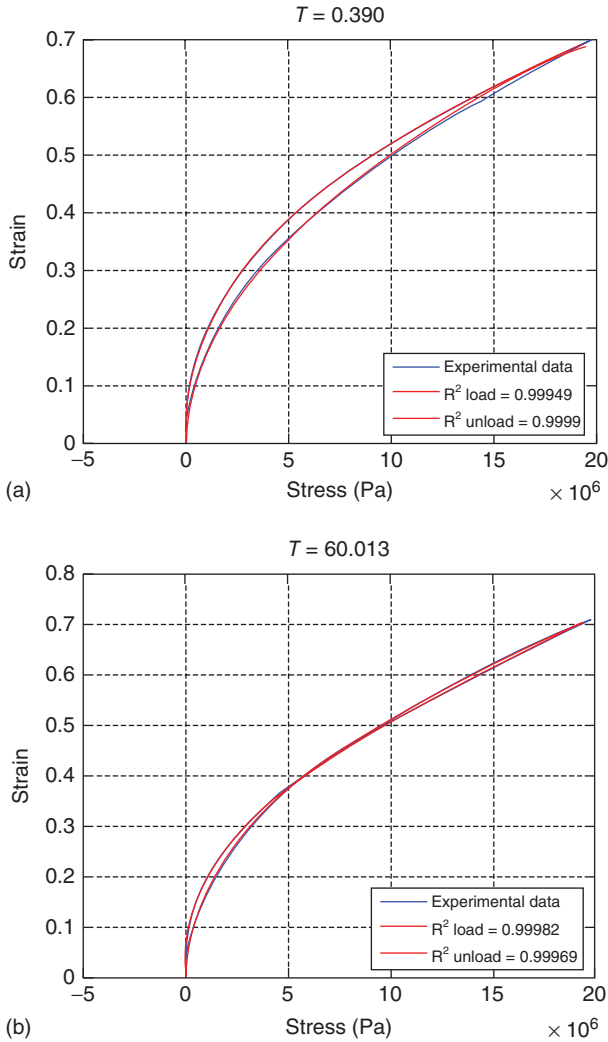


Figure 1.2 Stress–strain characteristics for sandstone from unconstrained quasistatic, uniaxial stress measurements. (a) The higher strain rate shows a difference between the

loading and unloading curves; (b) in a low strain rate experiment this hysteresis is much less apparent.

1.2.3

Moisture Content Variations

For completeness, it should be noted that careful and extensive macroscopic varying “humidity” measurements [16] hint at hysteresis, and there is extensive literature on the hysteresis seen in capillary condensation in soils as well. The book by Guyer and Johnson [3] discusses saturation and fluid content as a way of altering

the thermodynamic state of a rock, just as varying temperature can be thought of that way. However, varying moisture content and carefully quantifying it is much more difficult than varying temperature. It is also not so amenable to neutron scattering measurements, and thus these measurements are outside of the selected scope of this chapter.

1.2.4

Vibrational Excitation Variations

Finally, we mention an interesting applied field, introducing vibration as an applied field, resulting in a phenomenon called slow dynamics. In these experiments, the application of an external acoustic drive introduces a change of the sample's internal energy as manifested by a softening of its modulus. An experiment where the acoustic drive is repeatedly turned on and off and the conditioning and recovery is observed were reported in [17] for a wide variety of rocks and even concretes (see Figure 1.3). Conditioning and recovery of the sample back to its original elastic state and modulus is time dependent, similar to creep in that it has been shown to condition and recover as $\log(t)$ where t is time [18]. What is interesting is that slow dynamics and rate effects are seen even in very dry rocks under ultra high vacuum (T.W. Darling, personal communication, 2011; also discussed in [18]). Very thin layers of water are not necessarily fluid-like in a very dry rock, but they may still play an important role and experiments are being carried out to continue to explore these aspects. Slow dynamics experiments are worth mentioning because the simultaneous neutron

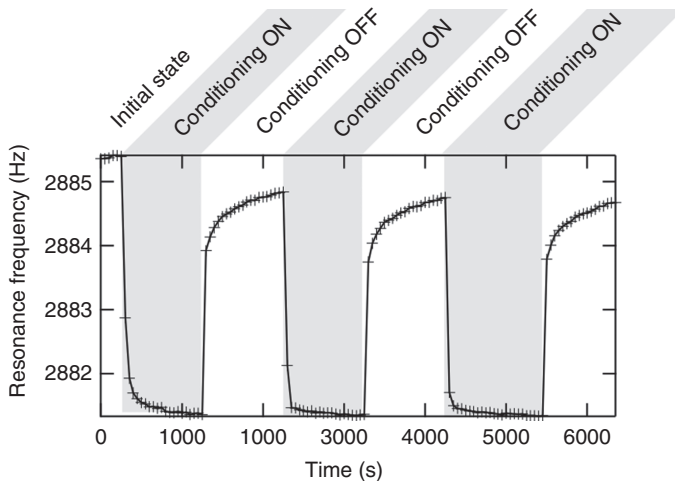


Figure 1.3 “Slow dynamics” – an accumulated mechanical effect using a symmetrical alternating strain acoustic drive. The elasticity of the rock, related to the resonant

frequency, diminishes rapidly initially, and then gradually a high amplitude drive is applied. The elasticity recovers in a similar way when the drive is removed.

diffraction including the following temperature measurements will mirror the same protocol, applying cooling and heating instead of applying an acoustic drive.

1.3

Motivation for Neutron Scattering Measurements

To learn about the mechanisms responsible for the interesting dynamic behavior just discussed, one must be able to probe and measure at very small scales. Systems with magnetic hysteresis have domains that can actually be observed flipping on a microscopic scale. Unfortunately, it is very difficult to microscopically watch what is going on or to understand what is causing the hysteresis observed in elastic/macroscopic measurements. Hence, there is a need for a probe/experiment that operates at a different (and much smaller) scale than these experiments discussed previously. It is also essential to simultaneously measure the macroscopic scale behavior, for example, stress–strain loops, slow dynamics, temperature, or humidity changes while using this probe.

A beam of neutrons traversing a rock can probe a smaller scale, the atomic (crystalline) structures, and dynamics of ordered *and* disordered materials such as crystals, glasses, and combinations thereof (e.g., perfect for sandstones). Since neutrons have no charge and scatter only from atomic nuclei, they penetrate deeply into most materials. This is important; the grains and bonds at the surface of a rock behave differently from the interior grains. Because other grains do not completely surround them and they are exposed to air and humidity, these surface grains are not representative of the bulk conditions that dominate the macroscopic effects observed. To learn about what is going on with the components deep *within* the sample, neutrons are absolutely essential.

Now contrast neutron with X-ray diffraction techniques—these have also been used to probe the atomic/crystalline structure of rocks. X-ray diffraction on small samples of *powdered* rocks is an effective way to determine chemical composition; moreover, some X-ray sources are energetic enough to penetrate and do microtomography on small intact samples to learn about vesicle and pore space density. X-rays, however, do not scatter effectively from the lighter elements such as oxygen, silicon, aluminum, calcium, sodium, potassium, and magnesium. These elements make up about 95% of the Earth's crust; oxygen and silicon alone make up about three-fourth of the weight of rocks on the Earth's surface. Neutron scattering cross-sections do not suffer from this atomic number dependence. Neutrons are thus an ideal choice to probe larger samples of intact rock at an atomic/crystalline scale (nanometers).

Neutron diffraction measurements with large intact samples allow simultaneous probing of the crystalline structure together with macroscopic measurements. Such was the aim of two sets of experiments described in this chapter, altering the pressure (stress–strain) and altering the temperature (temperature modulus), both done while simultaneously probing the crystalline structure with neutron scattering. One set of experiments made it possible to alter the stress on a sample and make stress–strain measurements while simultaneously watching the

behavior of the bulk of the crystalline content (the grains) in the rock. Another experiment, using a beamline with a very high neutron flux, allowed us to alter another external field, the temperature, while simultaneously tracking the behavior at the atomic scale.

Both the SMARTS (Spectrometer for MAterials Research at Temperature and Stress) and HIPPO (high-pressure preferred orientation) neutron time-of-flight (TOF) diffractometers are part of the neutron instrument suite at the Los Alamos Neutron Science Center (LANSCE). At the core of LANSCE is a half-mile long 800 MeV proton accelerator, serving multiple facilities, among them is the spallation neutron source of the Manuel Lujan Neutron Scattering Center [19].

The high-energy protons eject (“spall”) neutrons from the heavy nuclei in the spallation target. This pulse of fast neutrons is moderated to room temperature or lower, where the neutron de Broglie wavelengths are comparable to atomic spacings in solids. These neutrons leave the moderator at nearly the same time ($t=0$), but have a thermal distribution of energies (wavelengths). Shorter wavelength (faster) neutrons arrive first at the sample, followed by longer wavelengths. As these neutrons scatter from the sample, some wavelengths will fulfill the Bragg condition and produce a diffracted beam from a crystallite in the sample. The detected intensity of these diffracted beams as a function of time is also a function of wavelength, which provides the data for determining the atomic plane spacings within the crystallite. The random orientation and the large number of the crystallites fulfill the condition for *powder diffraction* where diffracted beams occur in a cone around the beam axis, so detectors intercepting any part of the cone will collect information on all the diffraction. We assume this condition to be true in our *intact* rock samples as well.

SMARTS is a third-generation neutron diffractometer optimized for the study of various engineering materials. It consists of an Instron load frame placed in such a way that simultaneous stress–strain and neutron diffraction measurements can be made under a variety of conditions. It was funded by DOE and constructed at the Lujan Center, coming online in the summer of 2001. SMARTS provides a range of capabilities for studying polycrystalline materials focusing on two areas: the measurement of deformation under stress (and extreme temperatures if desired), and the measurement of spatially resolved strain fields. SMARTS expands the application base of neutron diffraction to a wider range of engineering problems than previously possible, especially for the geomaterials (rocks) discussed in this chapter. With an extensive array of *in situ* capabilities for sample environments, it enables measurements on small to large (1 mm^3 to 1 m^3) samples. Permanently mounted alignment theodolites provide a simple and efficient way to position samples or equipment within 0.01 mm. *In situ* uniaxial loading on samples up to 1 cm in diameter with stresses from a few megapascals up to 2 GPa is routine. Sets of neutron diffraction measurements made on a suite of rocks [20] were taken at room dry conditions with maximum stresses up to 80 MPa; a subset of that work, the sandstones reported here, can withstand stresses up to about 50 MPa.

HIPPO is another third-generation neutron diffractometer that came online in 2001 funded primarily with support from the University of California and the US

DOE. It is unique in that its sample chamber is positioned very close (9 m) to the spallation target. The incoming thermal neutron flux on the sample is about $10^7 \text{ n}^{-1} \text{ cm}^{-2} \text{ s}^{-1}$ [21], delivered in pulses at a repetition rate of 20 Hz and typically collimated to a 10 mm diameter beam spot. The high count rate at HIPPO allows for dynamic measurements; atomic changes that occur on the order of minutes can be observed. We chose HIPPO to perform numerous step-temperature changes while simultaneously taking neutron diffraction measurements. Notable though is that in spite of high count rates at HIPPO, the low flux compared to the number of atoms in the irradiated volume (of the order of 10^{22} from Avogadro's number) and the energy of the order of 10 meV of thermal neutrons make effects like sample heating (or radiation damage) negligible. At the time, HIPPO was the only beamline in the world capable of these experiments, tracking the atomic/crystalline scale behavior of the rock during step-temperature changes. A vacuum-tight sample chamber in the HIPPO beamline of $\sim 1 \text{ m}^3$ accommodates a large variety of sample environments to expose vacuum dry samples to temperature [20], pressure [22], stress [23], magnetic fields, and combinations thereof as well as user-supplied sample environments. Our samples were mounted in a small helium-filled chamber (for heat transfer and, thus, were effective at room dry conditions). This inner sample chamber was then placed within the HIPPO sample chamber.

We now describe the results of *stress–strain measurements* on SMARTS [20] relevant to this chapter, and then follow that with a thorough discussion of the HIPPO experiment (unpublished), namely, *temperature modulus measurements* with simultaneous neutron diffraction data.

1.4

SMARTS: Simultaneous Stress–Strain and Neutron Diffraction Measurements

We used the SMARTS beamline to examine the *lattice* strain response of rock samples to an external cyclic pressure (stress) while simultaneously measuring the *macroscopic* strain response. All samples were cylinders of 13.4 mm diameter and 26.0 mm length, with flat, parallel ends ground perpendicular to the axis. X-ray diffraction was used to identify the solid components of the porous rocks, and the porosity was determined by the ratio of rock to mineral density. The SMARTS geometry is shown in Figure 1.4. The sample can be seen held horizontally between the conical anvils. (The copper tubing seen wrapped around one anvil is maintaining the temperature of that anvil.) The macroscopic strain is measured by a 12 mm (black) extensometer strain gauge, with knife edges held against the sample by elastic bands and hanging below the sample as seen in the figure. Data from detector 2 is used to determine the spacing of lattice planes, and these are compressed by the applied external stress. Lattice strains are determined from changes in the lattice spacings relative to an initial value. Since the sample was initially subject to a holding stress of around 4 MPa, the strain gauge was zeroed at that point and

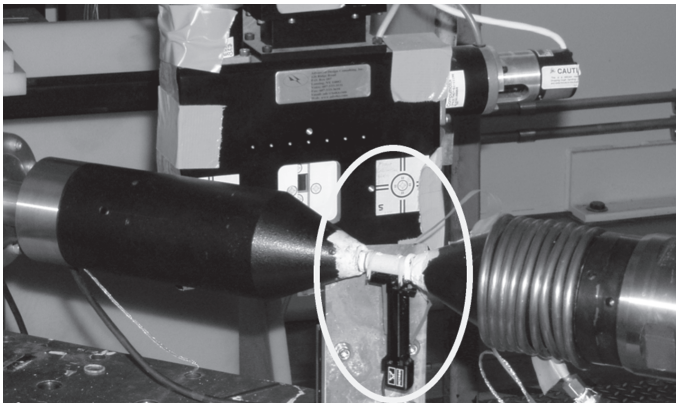
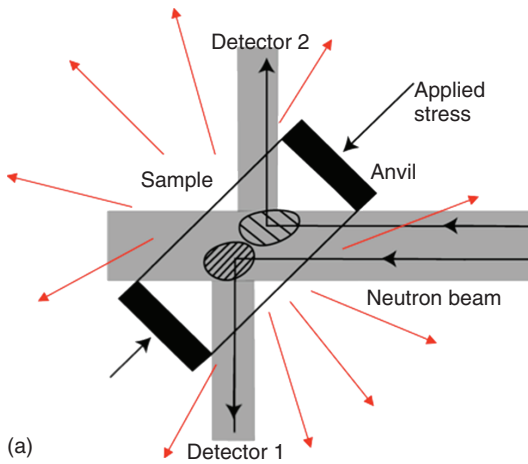


Figure 1.4 (a) The diagram shows neutrons scattered from a stressed sample (red arrows). Neutrons that are Bragg diffracted from atomic planes compressed by the axial stress are collected by detector 2, while

planes that deform radially diffract beams to detector 1. (b) The actual experiment in SMARTS is shown. Note the extensometer strain gauge attached under the sample to avoid direct exposure to the neutron beam.

the initial lattice spacings were measured. Initial experiments determined breaking stresses, and then further cycles on another sample were then limited to 70% of these values. Measurements were carried out at room dry ambient conditions (24–28 °C, 24% < relative humidity < 32%).

Macroscopic stress and strain values were recorded every 10 s throughout the experiment. The applied stress was changed between maximum and minimum values at 3 MPa min⁻¹, in an approximately triangle wave protocol. Neutron TOF diffraction spectra were collected for 15 min while holding the stress constant at fixed values, resulting in a slightly stepped load variation from the ideal triangle protocol.

Two perpendicularly directed lattice parameters (a , c) are needed to describe the trigonal unit cells of quartz. Rietveld analysis of the TOF spectra provides the spacing, and, more accurately, the *changes* in spacing (strain) of lattice planes perpendicular and parallel to the applied stress. In this chapter, only the neutron data for the response of a and c lattice parameters under compression (detector 2) are shown and compared with the macroscopic compression data.

The macroscopic stress–strain curves measured during the *in situ* loading measurements are shown in Figure 1.5. Neutron diffraction patterns for the Fontainebleau sandstone sample were recorded at compressive stresses of 5, 10, 15, 20, and 25 MPa followed by unloading by the same load levels. The macroscopic curve exhibits the expected nonlinear, hysteretic relation between stress and macroscopic strain (measured by the extensometer) similar to that shown in earlier work. The a and c lattice parameters – measured for the quartz grains at the holding stresses – are shown on the left (dashed) and both appear to be linear (elastic) within the margin of error. The slopes for a and c lattice parameters are slightly different because of the elastic anisotropy of quartz. The diffraction elastic constants, derived from linear fit to the data points, agree within error bars. The difference between macroscopic and microscopic maximal strain is striking. Continuum mechanics dictate agreement between macroscopic and microscopic strains, which is also observed in *in situ* neutron diffraction loading

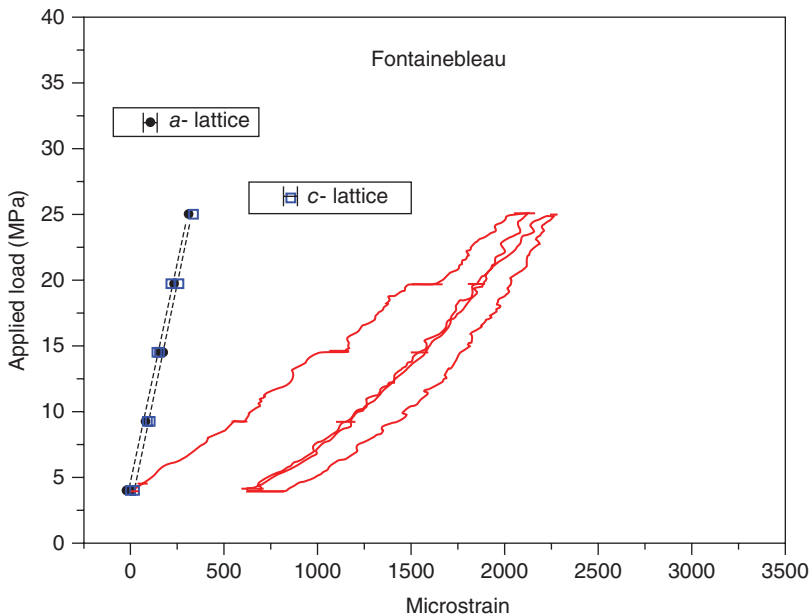


Figure 1.5 SMARTS data from the Fontainebleau sample – the red curve shows the macroscopic stress–strain behavior with initial conditioning followed by a repeating

hysteretic loop. The lattice planes compressed axially (detector 2) show a linear nonhysteretic strain response to the applied stress.

measurements of other materials such as steel [25, 26]. While these findings do not explain the observed macroscopic peculiarities, they appear to exclude that their origin is within the bulk of the quartz crystals. The data strongly suggest that it is what is not bulk crystallinity, namely, the bond system, which is responsible for the hysteresis in this and other sandstone samples examined.

1.5

HIPPO: Simultaneous Step-Temperature Modulus/Sound Speed and Neutron Diffraction Measurements

Our experiment follows the elastic behavior of a sandstone sample at both bulk and atomic lattice scales as temperature is cycled. We need to measure elasticity, temperature, and lattice parameters, and to control and change the temperature and environment of the sample. Ideally, we strove to measure the response of the rock to a step function change in the temperature, as for an electrical circuit analog.

We use the resonant frequency of the sample to determine the qualitative behavior of the elastic constants of the sample. Piezoelectric disks (PZT-5A) bonded to the ends of a cylindrical core act as driver and receiver (Figure 1.6) in a typical low-amplitude swept-frequency resonant ultrasound spectroscopy (RUS) [27] measurement. Type E (chromel–constantan) thermocouple junctions made with 0.003" diameter wires are glued into small holes of 2 mm deep near the ends

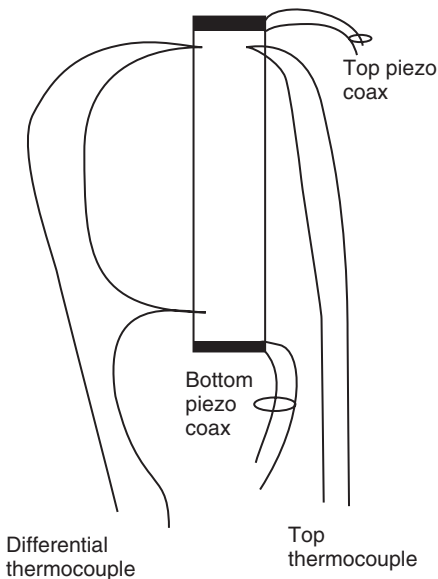


Figure 1.6 A diagram of the HIPPO sample with thermocouple junctions and piezoelectric disks. The thermocouple wires are kept away from the incident neutron beam to avoid spurious diffraction peaks.

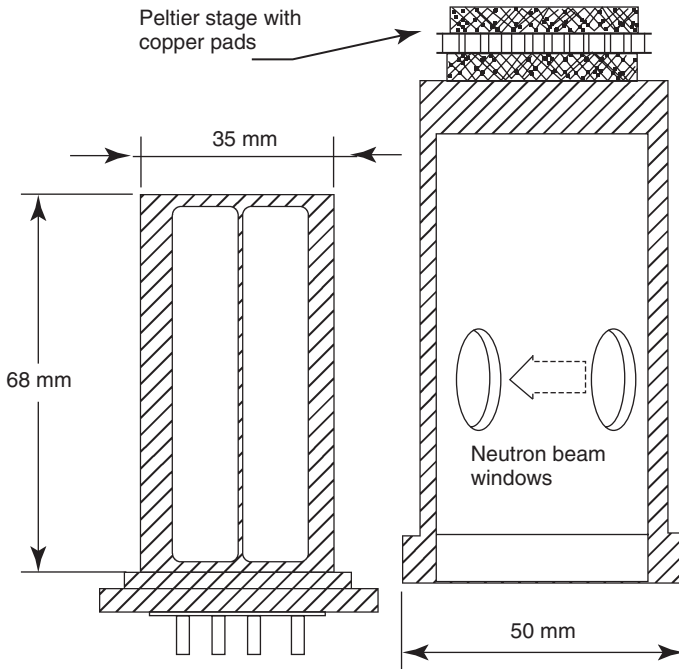


Figure 1.7 A diagram of the HIPPO sample holder and can. The sample is supported by threads inside the frame. The assembled unit is sealed with an atmosphere of helium gas inside to provide heat transfer from can to sample.

of the rock. The top thermocouple is measured against the internal reference of a Lakeshore model 325 controller, and a differential measurement across the sample is made and recorded on an HP voltmeter. Wire lengths were made as long as possible to avoid heat conduction between the junctions and from the base feedthroughs.

As noted in [3], temperature control of porous rock samples is complicated by low thermal diffusivity that makes changing the temperature of the rock uniformly problematic. In initial experiments, we found that large temperature gradients persisted indefinitely when heating by direct contact at one end. Our final design heats and cools an aluminum shell and uses helium exchange gas at atmospheric pressure to heat and cool the rock (see Figures 1.7 and 1.8).

1.5.1

Sample

The sample of interest is a 12.7 mm diameter core of Fontainebleau sandstone of length 55.6 mm. This is a relatively high porosity sample with $\phi = 23\%$. The grains are well rounded and in the size range 150–250 μm . This sandstone is very clean, being $>99.2\%$ quartz by XRD analysis. It also has one of the largest non-linear responses seen in acoustic tests [28], so making resonance measurements

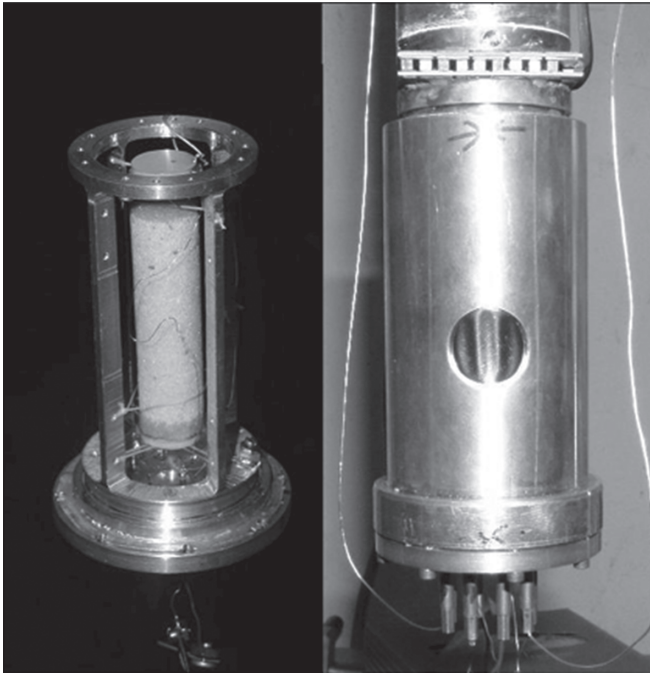


Figure 1.8 The HIPPO sample assembly – the neutron beam passes through Mylar windows in the can – which stretch under the helium pressure as the HIPPO well is evacuated, leaving wrinkles afterward.

at low amplitudes is essential. The sample is initially room dry, but the helium atmosphere for the measurements means water was being lost at a slow rate from the volume of the sample. Piezoelectric disks of PZT-5A material (in compression mode) are glued to each end with a thin copper foil for electrical connection at the junction. The glue used for the bonds is drawn in by capillary forces for a few millimeters into the sample at each end, as seen in Figure 1.8. This makes the sample a composite resonator of three components, dominated by the clean rock but with some glue-saturated rock and PZT elements at the ends. A finite element model (COMSOL) suggests that the observed resonances are consistent with a sound speed of approximately 1600 m s^{-1} in the clean rock. The gauge volume where the neutron beam probes the sample is in the central region of the clean rock.

1.5.2

Sample Cell

The sample cell provides the environment for the sample and must be able to operate inside the HIPPO experiment well. The cell is made up of two parts: each machined from a single piece of 6061 aluminum for maximum heat conductivity (see Figure 1.7). When assembled, the entire metal cell reaches a uniform

temperature in less than 100 s. An inner frame provides mounting space for the sample and its wire connections. Feedthroughs on the base of this frame pass electrical signals to the measurement apparatus. A standard Lakeshore curve-10 diode sensor is attached to the base of the frame to monitor the cell temperature. An outer can covers this frame and is sealed to it by an indium seal compressed by screws at the base. The top of the can has a single-stage Peltier unit, 1.5" square bolted to it with thick copper pads enabling us to solder the Peltier unit with low-temperature solder. The top of this Peltier assembly bolts to a 1.5" diameter aluminum rod that is both the mechanical support for the entire cell and the heat reservoir for the heating and cooling functions. The cell has windows – 15 mm diameter holes, sealed with aluminized 0.002" thick Mylar foil – placed so that the neutron beam can pass through the cell without hitting any of the solid aluminum parts. With the sample in place, the beam interacts with the central 1 cm of the sample. When the sample is mounted and all electrical connections have been made, the cell is assembled by displacing the air from the can with a flow of helium gas and inserting the frame and bolting the base to the can with the indium seal in place. The helium gas has a high conductivity and permeates the rock. This means heat transfer occurs not only through the gas from the can/frame to the outer surface of the rock but also through the He medium to the interior of the rock. This enhanced transfer enables us to approach a step function in temperature change, at least to timescales short compared to the nonlinear recovery times and to thermal diffusion times along the length of the sample. Although the HIPPO well is evacuated, we wrap the assembled cell in several layers of aluminized Mylar ("superinsulation") to provide radiation insulation against heat transfer with the well interior. The sample is supported inside the frame with dental floss thread, resting on a web below and with two tie points to keep the sample vertical. The frequency of vibration of the sample and this "springy" thread is below 200 Hz, so from the scale of the many kilohertz internal modes of the sample, it is essentially decoupled. A strain gradient possible due to gravity was shown to be negligible. Due to the pressure difference in the evacuated well, the windows suffer some stretching, leaving a corrugation when the cell is removed (Figure 1.8).

1.5.3

Procedure

LabVIEW[®] programs accumulate data from all the instruments. Measurements from the diode sensor on the can and the top thermocouple are recorded directly from the Lakeshore thermometers. The voltage across the differential thermocouples must be converted to a temperature difference using the known temperature of the nearby top thermocouple for one of the junctions, and so is post-processed. We have selected resonance modes near 26 kHz to monitor the elastic state of the sample. A DRS Inc. RUS system is used to sweep the drive and acquire the data. The swept-frequency data displays are also post-processed to extract the peak parameters by a Lorentzian profile-fitting procedure. The TOF diffraction

data are read as counts per neutron pulse and are stored and converted to $S(Q)$ plots. A test that the neutron beam is not hitting the cell is that no lattice spacings corresponding to aluminum are seen in the data. In order to maintain a good signal-to-noise level, neutron counts were accumulated for runs of 5 or 10 min, although a test demonstrated that adequate statistics could be acquired in only a 10 s run because of the high neutron flux available to HIPPO. Temperature control is achieved by controlling the current to the Peltier stage. Since the heat flow is bidirectional according to current and the thermal reservoir is the same for each – room temperature connected by the thick aluminum rod – we expect to have approximately symmetrical behavior for temperature changes around room temperature. The parameters for PID controllers to make a step function when the time constants are relatively long and the heat paths are not very high conductivity are difficult to determine: given the duration we expect for the sample to reach equilibrium, we controlled the changes manually with a variable current supply.

1.5.4

Results

Data were accumulated over a 17 h beam time run. The acoustic scan covered three compressional resonances corresponding to the second, third, and fourth modes (“Pochhammer” modes) at 22, 35, and 47 kHz approximately at room temperature. These modes are effectively driven by the large compression mode transducers. Scans were taken every minute at a drive amplitude as small as possible to avoid memory or slow dynamics effects – but large enough to be confident of the peak parameters. A sample scan is shown in Figure 1.9. The best-fit Lorentzian

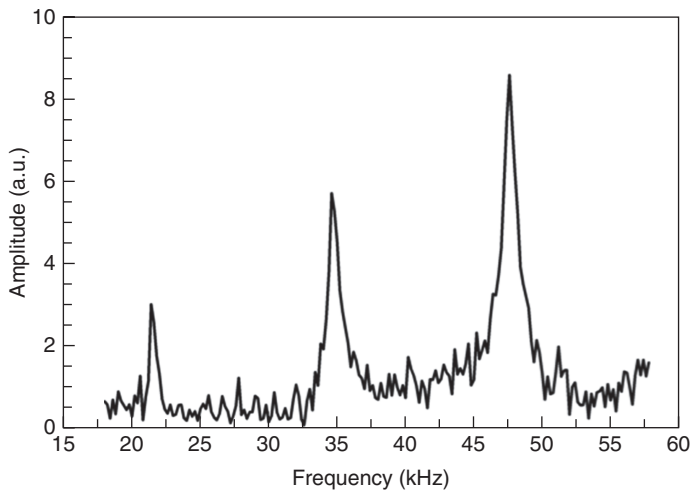


Figure 1.9 The first three longitudinal vibration modes of the Fontainebleau sample. To avoid slow dynamical effects, we used the lowest amplitude drive that still gave a good signal-to-noise ratio.

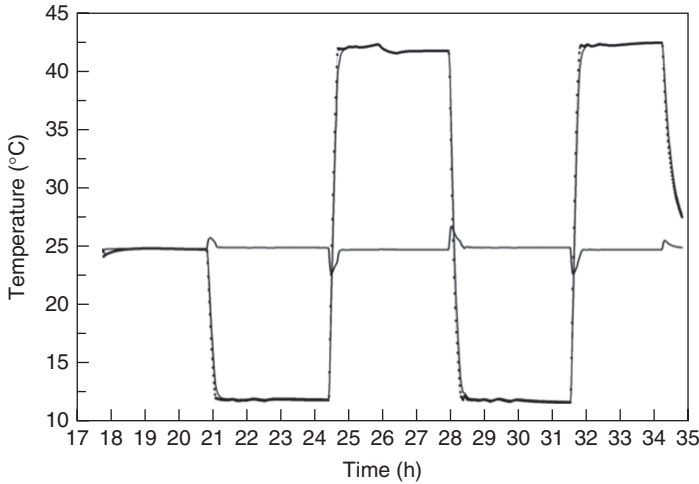


Figure 1.10 The temperature protocol for the experiment. The top and bottom sample temperatures are shown (dotted and continuous) almost overlapping with a swing of about 30 K. The difference plot near the axis shows a small difference resolving to zero in about 15 min after each applied change. We avoided approaching the freezing point of water.

lineshape parameters show the effect on these peaks as temperature changes. The temperature of the sample cell was taken through two complete cycles where the temperature ranged from about 12 to 43 °C around a room temperature of 25 °C. The cell responds rapidly to the Peltier heat flow, but even with the He exchange gas the rock temperature and the gradient respond more slowly, taking 15–20 min to reach a steady state. The cell, rock, and differential (top to bottom) temperatures are shown in Figure 1.10. The temperature used in all the data plots corresponds to the temperature at the center of the sample, evaluated from the top and differential temperatures. This is quite accurately (within ± 0.3 °C) the temperature of the neutron gauge volume and is a good average for the overall acoustic response being within 1 °C in the 20 min after a temperature change and within 0.1 °C otherwise. Neutron scattering data were accumulated in 10 min runs for the first 13 runs and at 5 min runs thereafter to the end of the experiment. As can be seen from Figure 1.11, the circles representing the unit cell volume evaluated from the Rietveld lattice parameter refinement, scaled to the temperature swing, follow the rock average temperature curve accurately, albeit with a small spread of values. The absolute value of the unit cell volume is a little larger than standard values due to calibration deviations. These data confirm that the crystalline volume of the rock is responding essentially only to thermal expansion in an expected way with the temperature changes. As noted in the SMARTS data for uniaxial compression, this does not necessarily dictate the mechanical response of the entire sample.

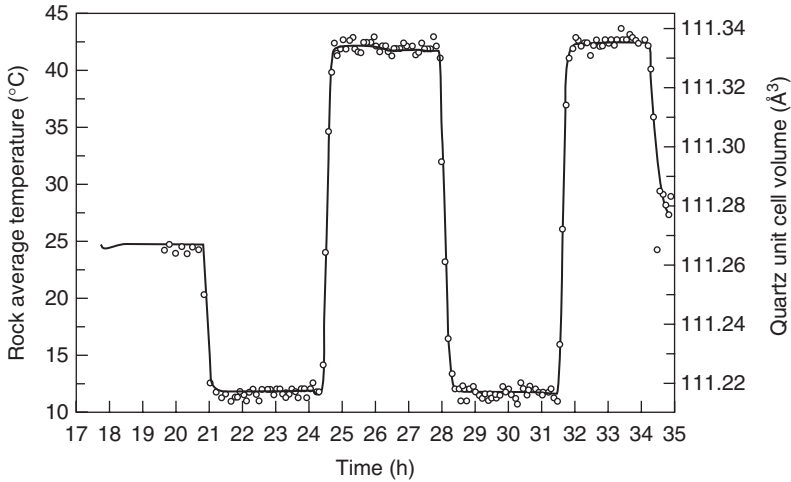


Figure 1.11 The average (top + bottom)/2 of time. The lattice in the majority crystalline component in the grains changes essentially temperature of the sample (continuous line) and the neutron diffraction derived atomic unit-cell volume (open circles) as a function instantaneously to follow the temperature change.

The Lorentzian fitting program gives amplitude, center frequency, and width parameters for each peak. There is also phase information, but since the resonances do not overlap this information is not used. The quality factor “*Q*” of the sample resonance may be determined by dividing the center frequency by the width. Fits in general were good, given the signal to noise seen in Figure 1.9. Since these modes are of the same kind and the wavelengths are large compared to the microstructure of the sample, we expect the behavior of their parameters to be similar. It is shown in Figure 1.11 for the center frequency changes that this is indeed so, and is also true for the amplitude and width data. The highest frequency peak (mode 4) will be used to represent the behavior of all the peaks and the sample. Figure 1.12 displays the center frequency and the temperature variation for the sample. Several characteristics are worth noting: the initial cycle is different from the subsequent cycle, a “conditioning” behavior seen in many tests on rocks including standard stress–strain tests; the frequency is higher when the sample is colder, as expected, but an initial dip occurs for *both* temperature increases and decreases, followed by an increase; and the frequency lags considerably behind the temperature change. This last point represents the hysteretic response of the rock – the dry conditions and high permeability suggest that there is insufficient liquid to produce a viscous drag and the gas environment is too light and mobile to influence the mechanical response. The strain in the crystallites responds essentially instantaneously to temperature change, suggesting that the delay in the overall mechanical response of the sample is dominated by solid components that are not a large component of the coherent neutron scattering signal.

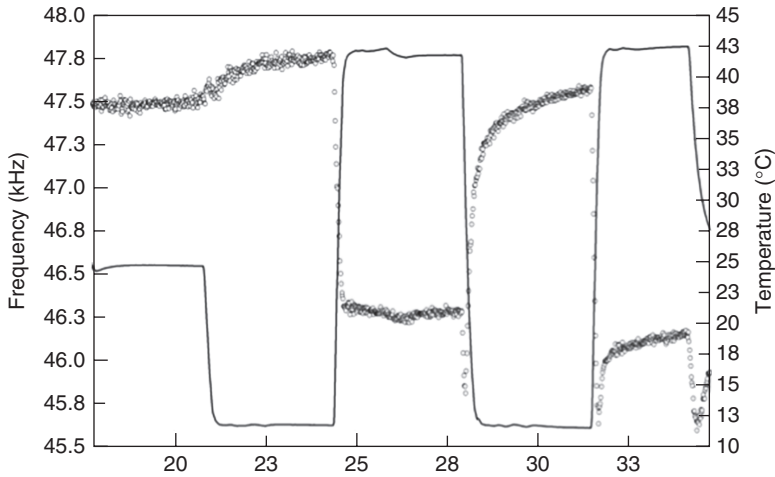


Figure 1.12 The sample average temperature (continuous line) and the frequency of the third longitudinal mode (open circles) as a function of time. The overall change agrees with expected changes in the elasticity (higher T and lower modulus), but

the form does not follow the temperature, showing a gradual recovery after initial rapid change. Major differences with slow dynamics (Figure 1.3) are the downward dip at each temperature change and the “recovery-like” curve at both constant temperatures.

The width of mode 4 can be used to evaluate the change in Q of the sample with temperature, as shown in Figure 1.13. The Q of all three modes is between 20 and 50 over the entire temperature range.

The Q is, in general, higher at lower temperatures but again the dip-and-recover characteristic can be seen – it is also in the width alone, demonstrating that there is a jump in the damping at each temperature change that diminishes with approximately the same time behavior as the center frequency.

Figure 1.14 shows center frequency plotted against temperature. This displays a typical hysteresis loop with two main features imposed on it. First, there is a conditioning effect – a removal of a transient property – that is not complete at the end of the experiment. This conditioning makes the loop decrease in frequency over time, but eventually leaves the sample in a state where the loop repeats – this experiment did not reach that state. Second, the dip-and-recover being similar at both signs of temperature change leads to the loop becoming a “bow-tie.” The crossing of these is seen at about 35 °C on the final cycle. This feature is not often observed in quasistatic tests, but is common in experiments where the excitation can be changed on shorter timescales than the recovery.

1.5.5

Comparison/Reference Measurements

A measurement on a known sample of the same size as these Fontainebleau samples – steel – was made to ensure that the results of the three-pronged (acoustic,

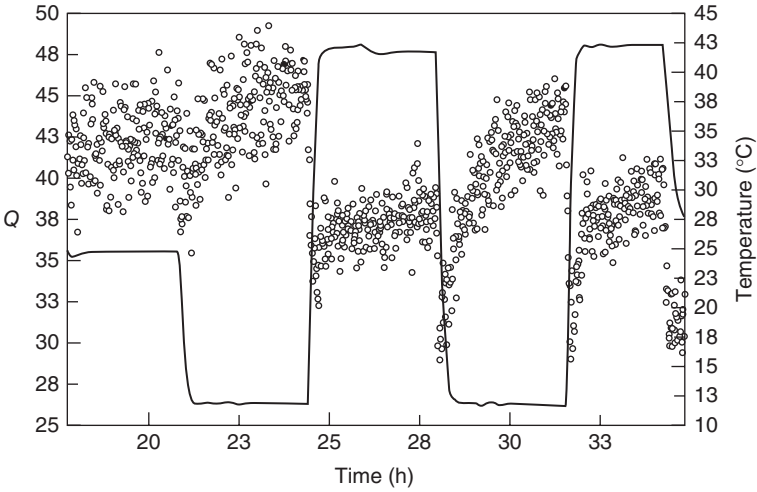


Figure 1.13 The sample average temperature (continuous line) and the Q of the third longitudinal mode (open circles) as a function of time. Although there is more scatter in this data, the features noted for the center frequency (Figure 1.12) also appear in the Q .

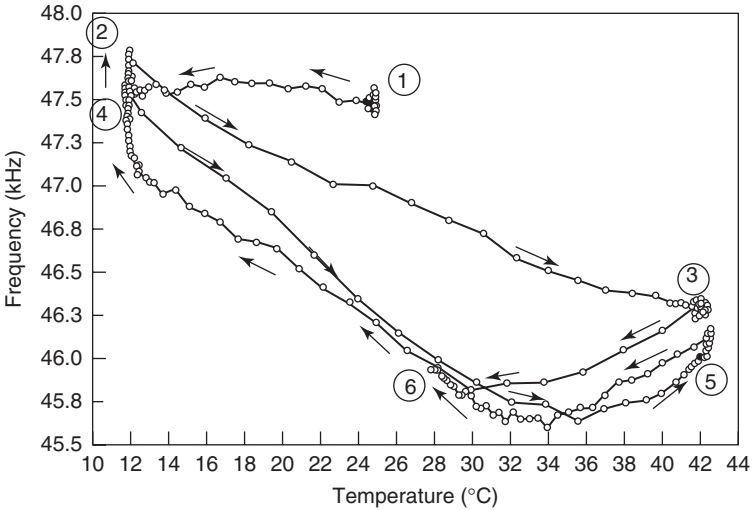


Figure 1.14 Hysteresis loops in the temperature–frequency characteristic from Figure 1.12. The line merely joins the data points, to help follow the path, labeled 1–6. After the first cycle, the loop changes toward a “bow-tie” shape, caused by the similar “recovery-like” response at both the high and low temperatures.

thermal, and neutron) approach made sense. Figure 1.15 shows the combined results for the center frequency of a compressional resonance, the fitted unit cell volume, and the applied temperature profile. The frequency plot has been inverted since we expect lowering the temperature to increase the frequency, and all are

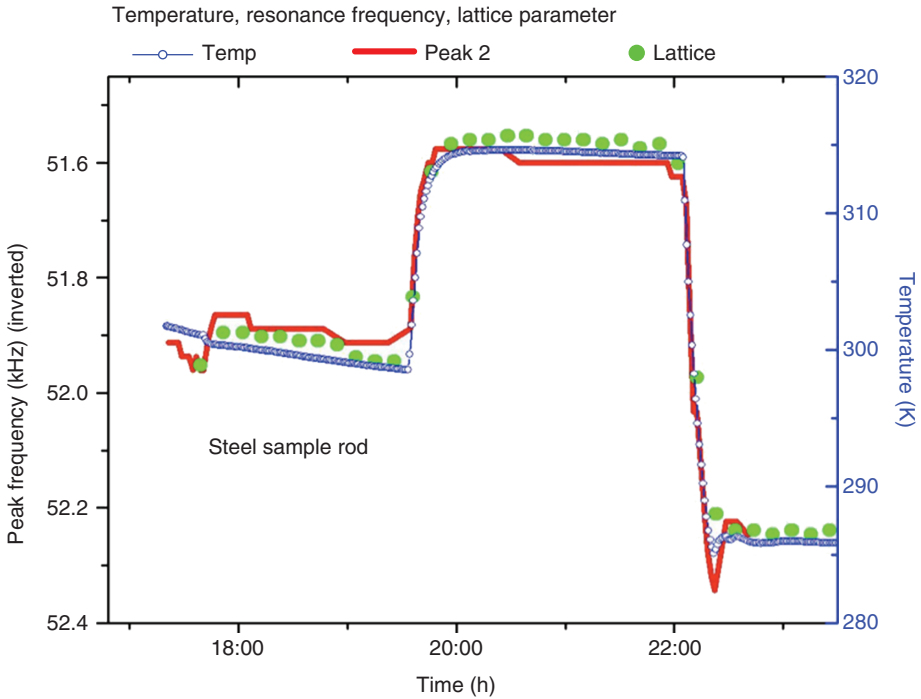


Figure 1.15 A plot showing that in a known nonporous sample (steel), the temperature, the frequency of a resonant mode (inverted to correspond to the T change), and the atomic lattice spacing all correspond closely.

scaled to a common step height. For steel, with its high thermal diffusivity, the lattice and the whole body resonances respond identically to the temperature step. A later acoustic temperature measurement (no lattice information) was made on a sample of Novaculite, a very low porosity, pure dense quartzite. Figure 1.16 shows data plots matching those of Figures 1.12 and 1.14, respectively, for the Fontainebleau. Although the materials for both are $>99\%$ SiO_2 , the porosity of the sandstone gives grains a room to displace and rotate, thus generating a highly nonuniform strain distribution. The high strains in the (also nonuniform) cementation drive the processes responsible for the mechanical hysteresis.

1.6

Discussion and Conclusions

We have made a system that can make a relatively fast change in the temperature of a porous rock sample and then measure the time lag for the elastic properties to change. The longitudinal resonance frequency follows the change in the elasticity and can be measured with high accuracy, even in intrinsically low- Q systems such as sandstones. We find that the speed of the temperature change is limited by three

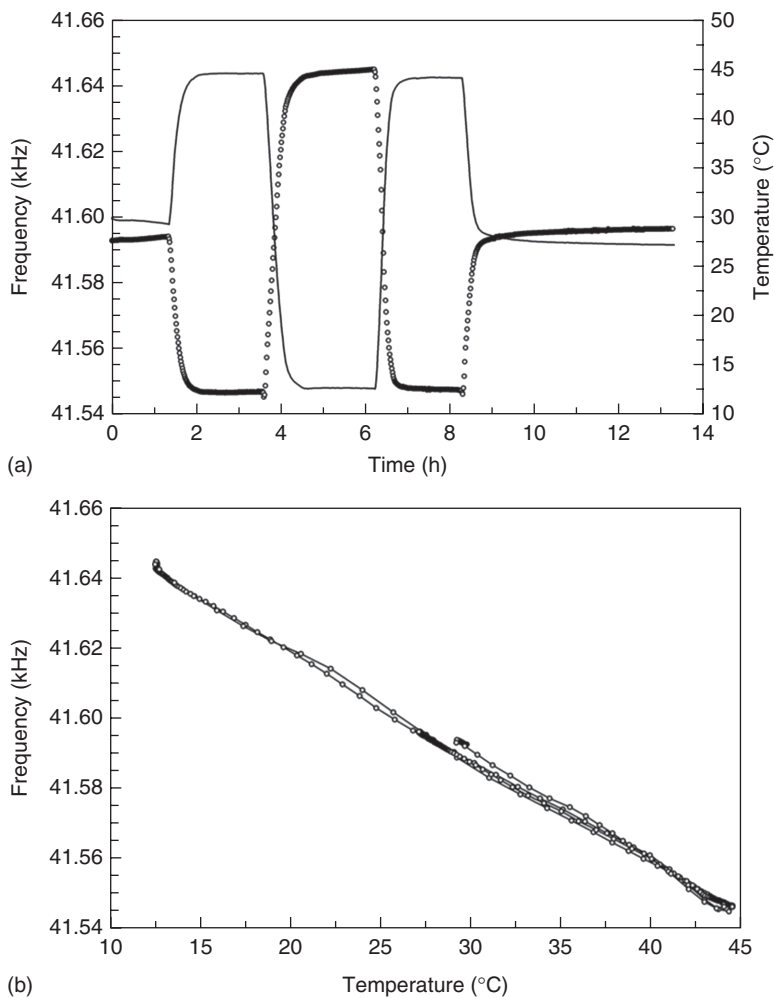


Figure 1.16 The sample average temperature (continuous line) and the frequency of a longitudinal mode (open circles) as a function of time for a sample of Novaculite (a) and the temperature–frequency

characteristic (b). The temperature control was not as good as for the same experiment on Fontainebleau (Figures 1.12 and 1.14), but the behavior of this dense quartzite is clearly nonhysteretic.

factors: the power of the Peltier stage; the conductivity of the sample can and He exchange gas; and the thermal diffusivity of the sample. We believe that the helium gas permeates the rock and provides a high conductivity path to the interior of the rock, enabling it to reach thermal equilibrium more quickly than in vacuum. The rapidity with which the average lattice constant of the sample crystallites changes seems to bear this out; a large gradient would broaden the diffraction peaks. The aluminum can and frame are also of high conductivity, so it seems we might have made a more rapid step by increasing the power of the Peltier stage heat pump.

Observation shows that the time taken for the rock to attain elastic equilibrium after a given temperature step is several hours, so the temperature change over an interval of ~ 15 min is relatively fast. Every element of material will be expanding or contracting according to the thermal expansion coefficients of quartz – the large crystallite volume matches this quickly, but other data [29] suggest that the overall expansion is close to 30% of the quartz (or dense quartzite) value implying that the grains expand or rotate into the pore space, placing large strains in the cementation. *We believe that the combined neutron diffraction results place the hysteretic behavior in the cementation*, a result similar to that reported for the SMARTS stress–strain data in [20].

The cement is generally a complex structure [1] – layered with possibly different morphologies, water content, and crystallinity in each layer – so a large number of potential strain-dependent energy structures might produce the microscopic hysteretic effects. Recent results with *very dry* Berea sandstone suggest that fluid water is not necessary for nonlinear or hysteretic effects, but monolayers of water within or on the cementation may still be active.

Finally, a note about the final external applied field was considered, applying an acoustic field to the rock while taking neutron diffraction data. While macroscopic measurements are relatively easy to track, the applied strain magnitudes are still small when compared with the strains produced in a stress–strain or change of temperature measurement. Nevertheless, an attempt was made to look for changes in the bulk crystalline structure of the rock by taking neutron TOF data during a few cycles of applied acoustic field and then turning that field off and repeating. No evidence of any changes was observed in the Rietveld analysis.

Acknowledgments

We gratefully acknowledge the support of the US Department of Energy through the LANL/LDRD Program for this work. One of us (TWD) would additionally like to acknowledge the support from the DOE's Office of Basic Energy Sciences and Office of Geosciences under grant #DE-FG02-11ER16218 for some of this work.

References

1. Haddad, S.C., Worden, R.H., Prior, D.J., and Smalley, P.C. (2006) Quartz cement in the Fontainebleau sandstone, Paris basin, France: crystallography and implications for mechanisms of cement growth. *J. Sediment. Res.*, **76**, 244–256.
2. Bourbie, T., Coussy, O., and Zinszner, B. (1987) *Acoustics of Porous Media*, *Institute Francais du Petrole Publications*, Editions Technip, Paris, (1986) (English translation).
3. Guyer, R.A. and Johnson, P.A. (2009) *Nonlinear Mesoscopic Elasticity*, Wiley-VCH Verlag GmbH, Print, ISBN: 9783527407033, Online ISBN: 9783527628261, doi: 10.1002/9783527628261.
4. TenCate, J.A. and Shankland, T.J. (1996) Slow dynamics in the nonlinear elastic

- response of Berea sandstone. *Geophys. Res. Lett.*, **23** (21), 3019–3022.
5. Adams, F.D. and Coker, E.G. (1906) *An Investigation into the Elastic Constants of Rocks, More Especially with Reference to Cubic Compressibility*, Carnegie Institute of Washington, Publication No. 46.
 6. Boitnott, G.N. (1993) Fundamental observations concerning hysteresis in the deformation of intact and jointed rock with applications to nonlinear attenuation in the near source region. Proceedings of the Numerical Modeling for Underground Nuclear Test Monitoring Symposium. Report LA-UR-93-3839, Los Alamos National Laboratory, p. 121.
 7. Hilbert, L.B. Jr., Hwong, T.K., Cook, N.G.W., Nihei, K.T., and Myer, L.R. (1994) in *Rock Mechanics Models and Measurements Challenges from Industry* (eds P.P. Nelson and S.E. Laubach), A. A. Balkema, Rotterdam, p. 497.
 8. Nihei, K.T., Hilbert, L.B. Jr., Cook, N.G.W., Nakagawa, S., and Myer, L.R. (2000) Frictional effects on the volumetric strain of sandstone. *Int. J. Rock Mech. Min. Sci.*, **37**, 121–132.
 9. Holcomb, D. (1981) Memory, relaxation, and microfracturing in dilatant rock. *J. Geophys. Res.*, **86** (B7), 6235–6248.
 10. McCall, K.R. and Guyer, R.A. (1994) Equation of state and wave propagation in hysteretic nonlinear elastic materials. *J. Geophys. Res.*, **99**, 23887.
 11. Guyer, R.A., McCall, K.R., Boitnott, G.N., Hilbert, L.B. Jr., and Plona, T.J. (1997) Quantitative implementation of Preisach-Mayergoyz space to find static and dynamic elastic moduli in rock. *J. Geophys. Res.*, **102**, 5281–5293.
 12. Claytor, K.E., Koby, J.R., and TenCate, J.A. (2009) Limitations of Preisach theory: elastic aftereffect, congruence, and end point memory. *Geophys. Res. Lett.*, **36**, L06304.
 13. Ide, J.M. (1937) The velocity of sound in rocks and glasses as a function of temperature. *J. Geol.*, **XLV**, October–November issue, 689–716.
 14. Ulrich, T.J. and Darling, T.W. (2001) Observation of anomalous elastic behavior in rock at low temperatures. *Geophys. Res. Lett.*, **28** (11), 2293–2296.
 15. Ulrich, T.J. (2005) Thesis. University of Nevada, Reno.
 16. Clark, V.A. (1980) Effect of volatiles on seismic attenuation and velocity in sedimentary rocks. PhD dissertation. Texas A&M, University Microfilms International, 8101583.
 17. TenCate, J.A., Smith, E., Byers, L.W., and Shankland, T.J. (2000) in *CP524, Nonlinear Acoustics at the Turn of the Millennium: ISNA 15* (eds W. Lauterborn and T. Kurz), American Institute of Physics, pp. 303–306.
 18. TenCate, J.A. (2011) in *Pure and Applied Geophysics, Special Issue on Brittle Deformation* (eds Y. Ben-Zion and C. Sammis), PAGEOPH Topical Volumes, Birkhauser, pp. 65–74.
 19. Lisowski, P.W. and Schoenberg, K.F. (2006) The Los Alamos Neutron Science Center. *Nucl. Instrum. Methods Phys. Res., Sect. A*, **562**, 910–914.
 20. Darling, T.W., TenCate, J.A., Brown, D.W., Clausen, B., and Vogel, S.C. (2004) Neutron diffraction study of the contribution of grain contacts to nonlinear stress-strain behavior. *Geophys. Res. Lett.*, **31**, L16604.
 21. Ino, T., Ooi, M., Kiyonagi, Y., Kasugai, Y., Maekawa, F., Takada, H., Muhrer, G., Pitcher, E.J., and Russell, G.J. (2004) Measurement of neutron beam characteristics at the Manuel Lujan Jr. neutron scattering center. *Nucl. Instrum. Methods Phys. Res., Sect. A*, **525**, 496–510.
 22. Zhao, Y., Zhang, J., Xu, H., Lokshin, K.A., He, D., Qian, J., Pantea, C., Daemen, L.L., Vogel, S.C., Ding, Y., and Xu, J. (2010) High-pressure neutron diffraction studies at LANSCE. *Appl. Phys. A*, **99**, 585–599.
 23. Hartig, C., Vogel, S.C., and Mecking, H. (2006) In-situ measurement of texture and elastic strains with HIPPO–CRATES. *Mater. Sci. Eng. A*, **437**, 145–150.
 24. Vogel, S.C. and Priesmeyer, H.-G. (2006) in *Neutron Scattering in Earth Sciences, Reviews in Mineralogy and Geochemistry*, vol. 63 (ed. H.-R. Wenk), pp. 27–57.
 25. Clausen, B., Lorentzen, T., and Leffers, T. (1998) Self-consistent modeling of the plastic deformation of FCC polycrystals

- and its implications for diffraction measurements of internal stresses. *Acta Mater.*, **46**, 3087.
26. Clausen, B., Lorentzen, T., Bourke, M.A.M., and Daymond, M.R. (1999) Lattice strain evolution during uniaxial tensile loading of stainless steel. *Mater. Sci. Eng.*, **A259**, 17.
 27. Migliori, A. and Sarrao, J.L. (1997) *Resonant Ultrasound Spectroscopy*, John Wiley & Sons, Inc.
 28. Johnson, P.A., Zinszner, B., and Rasolofosaon, P.N.J. (1996) Resonance and nonlinear elastic phenomena in rock. *J. Geophys. Res.*, **101** (B5), 11553–11564.
 29. Touloukian, Y.S., Judd, W.R., and Roy, R.F. (1981) *Physical Properties of Rocks and Minerals*, Thermophysical Data for High Porosity Sandstone, Purdue Research Foundation.

